Dielectric properties, electric-field-induced polarization and strain behavior of Lead Zirconate Titanate-Strontium bismuth Niobate ceramics

Orapim Namsar[1] · Anucha Watcharapasorn[1,2] · Mark Hoffman[3] · Julia Glaum[3] ·
Sukanda Jiansirisomboon[4]

Abstract The dielectric properties and electric-field-induced polarization and strain behavior of $(1-x)$PZT-xSBN (x ranged from 0 to 1.0 weight fraction) ceramics prepared by a conventional mixed-oxide method were investigated. The dielectric properties indicated that the dielectric constant of PZT could be enhanced with small addition of SBN ($x = 0.1$). From the polarization hysteresis loop measurements, it was found that the ferroelectric properties of nominal PZT-SBN ceramics changed strongly from the normal ferroelectric in PZT-rich ceramics to the paraelectric character in SBN-rich compositions. The strain hysteresis loops of nominal PZT-SBN under bipolar electric field loading suggested that the butterfly curve was observed in some compositions ($0 \leq x \leq 0.3$ and pure SBN ceramic). This research clearly showed the significance of SBN in controlling the electrical properties of nominal PZT-SBN ceramics.

✉ Sukanda Jiansirisomboon
sukanda.jian@cmu.ac.th

[1] Department of Physics and Materials Science, Faculty of Science, Chiang Mai University, Chiang Mai 50200, Thailand

[2] Materials Science Research Center, Faculty of Science, Chiang Mai University, Chiang Mai 50200, Thailand

[3] School of Materials Science and Engineering, University of New South Wales, Sydney, NSW 2052, Australia

[4] School of Ceramic Engineering, Suranaree University of Technology, Nakhon Ratchasima 30000, Thailand

1 Introduction

Ferroelectric materials have attracted considerable attention because of their possible uses in electronic devices such as nonvolatile random access memories (NVRAM), capacitors and actuators [1]. Isotropic perovskite structure and bismuth layered structure compounds are the two most important materials employed in these applications. Perovskite-structure compounds such as $Pb(Zr_{0.52}Ti_{0.48})O_3$ (PZT) show excellent ferroelectric properties with large remanent polarization and small coercive field [2] but they exhibit a rather poor fatigue resistance [3]. The bismuth layered perovskite compounds i.e. $SrBi_2Nb_2O_9$ (SBN) and $SrBi_2Ta_2O_9$ (SBT) exhibit excellent fatigue characteristics as compared to those of PZT [4]. However, the major problems of these bismuth layered perovskite ferroelectrics include small remanent polarization and high processing temperature [5]. Therefore, many research groups have attempted to combine the superior ferroelectric properties of PZT and fatigue-free properties of SBT in a form of mutilayer thin films [6, 7]. Many previous works reported that the binary film systems had better ferroelectric and dielectric properties over those of pure PZT thin films. However, fundamental research on a combination of PZT and bismuth layered compounds in a form of bulk ceramic is quite scarce. Therefore, this research aims to fabricate new ceramic systems based on PZT-SBN. A series of ceramics with formula $(1-x)$PZT-xSBN (when $x = 0, 0.1, 0.3, 0.5, 0.7, 0.9$ and 1.0 weight fraction) were prepared. The ceramics were characterized particularly in terms of phase evolution and its relationship to strain behavior, dielectric and ferroelectric properties.

2 Experimental

The conventional solid state reaction method was employed to prepare the ceramics with formula $(1-x)Pb(Zr_{0.52}Ti_{0.48})O_3$-

xSrBi$_2$Nb$_2$O$_9$ or (1-x)PZT-xSBN where x = 0, 0.1, 0.3, 0.5, 0.7, 0.9 and 1.0 weight fraction. PZT and SBN were synthesized separately. The raw materials of PbO (99 %, Riedel-de Haën), ZrO$_2$ (99 %, Riedel-de Haën), TiO$_2$ (99 %, Riedel-de Haën) were weighed according to Pb(Zr$_{0.52}$Ti$_{0.48}$)O$_3$ composition. The mixture of raw materials was ball milled in alcohol for 24 h using zirconia balls. After that, the powder mixture was calcined at 800 °C for 2 h to form the perovskite PZT. SBN was similarly prepared from mixed SrCO$_3$ (98 %, Aldrich), Bi$_2$O$_3$ (99.9 %, Aldrich) and Nb$_2$O$_5$ (99.9 %, Aldrich) powders which were reacted at a calcination temperature of 950 °C for 3 h. Then, the PZT and SBN powders with different relative weight fraction were wet mixed for 24 h in a plastic jar with zirconia balls and ethanol. The dried powders were pressed into pellets with 10 mm in diameter. The green pellets were then placed in a sealed alumina crucible. These pellets were covered with powder having the same composition to avoid compositional deviation from PbO and Bi$_2$O$_3$ volatilization during sintering at 1050 °C for 3 h with a heating/cooling rate of 5 °C/min. The amount of excess powder was about 5 g per crucible.

Phase characterization of (1-x)PZT-xSBN ceramics was carried out using X-ray diffractometry (XRD, Phillip Model X-pert). The polarization-electric field (P-E) and strain-electric field (S-E) loops were measured at a frequency of 50 Hz using an aixACCT TF2000HS analyzer equipped with a laser interferometer. Dielectric properties were measured at room temperature with a measurement frequency of 1 kHz using the LCR Hitester (Agilent, E4980A).

3 Results and discussion

X-ray diffraction patterns of (1-x)PZT-xSBN ceramics after sintering at 1050 °C for 3 h are shown in Fig. 1(a). The XRD pattern of the PZT sample was identified as a single-phase pattern with a perovskite structure having tetragonal symmetry while the SBN ceramic was found to be a bismuth layered structure with an orthorhombic symmetry. The addition of 0.1SBN into PZT caused a shift of the PZT peaks to higher angles while a newly formed phase started to appear. X-ray peak matching procedure indicated that this new phase was found to have a pattern very similar to the standard data of the Pb$_2$(Nb$_{1.33}$Ti$_{0.66}$)O$_{6.66}$ (PNT) whose structure is cubic with space group Fd3 m (JCPDS file no. 74–0660). Similar results have been observed by Yang et al. [8] in the PZT-Bi$_4$Ti$_3$O$_{12}$ system. They found that the new stable phase of composition PbBi$_4$Ti$_4$O$_{15}$ coexisted with the PZT matrix phase. This confirmed that a chemical reaction and dissolution between the perovskite PZT and bismuth layered SBN occurred during the sintering process. During the dissolution process, it was expected based on ionic size that Sr^{2+} (r_{Sr}^{2+} = 1.18 Å) or Bi^{3+} (r_{Bi}^{3+} = 1.03 Å) substituted for Pb^{2+} (r_{Pb}^{2+} = 1.19 Å), and
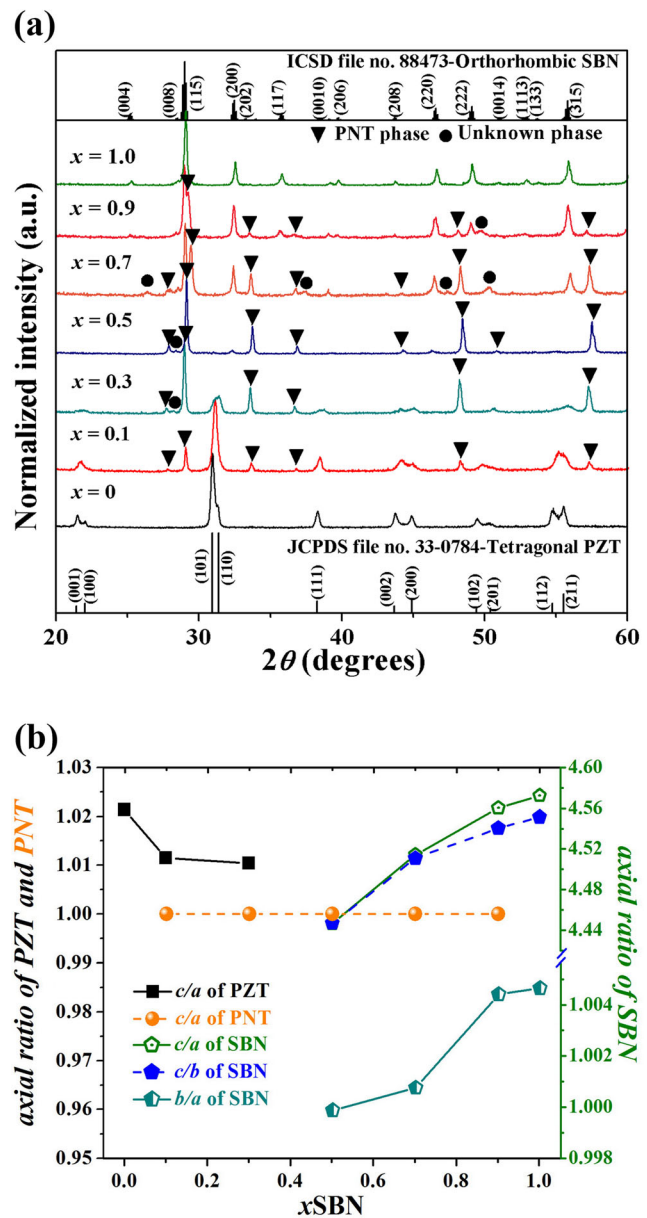
Fig. 1 (a) X-ray diffraction patterns of (1-x)PZT-xSBN ceramics (b) Axial ratio of (1-x)PZT-xSBN ceramics

Nb^{5+} (r_{Nb}^{5+} = 0.64 Å) ion substituted for Ti^{4+} (r_{Ti}^{4+} = 0.605 Å) or Zr^{4+} (r_{Zr}^{4+} = 0.72 Å) [9] in PZT. This ionic substitution resulted in a shift of all PZT diffraction peaks towards higher angles. For x = 0.3, the intensity of the PNT peaks increased rapidly while the intensity of the PZT peaks sharply decreased. For the composition x = 0.5, the pattern indicates that peaks of PNT became the major phase with the appearing SBN as a minor phase while the peaks of the PZT phase completely disappeared. An increase in SBN content from x = 0.7 and 0.9 led to a gradual reduction of PNT peak intensity and the shift of SBN peaks to lower angles with a continuous increase in intensity. This peak shift implied the expansion of the unit cell of the SBN phase. With careful

phase characterization, it was shown that some extra peaks of unknown phase were also present in the composition range of $0.3 \leq x \leq 0.9$, which were indicated by black circles in Fig. 1(a). Furthermore, as shown in Fig. 1(b), it was observed that the variation of axial ratio of PZT, PNT and SBN phases in nominal PZT-SBN ceramics showed a strong reduction in c/a after the incorporation of a small amount of SBN ($0.1 \leq x \leq 0.3$) compared to PZT without SBN addition. This implied that the ions from SBN dissolved into the PZT phase creating the shift in the XRD peaks mentioned previously. On the other hand, the addition of PZT into SBN (in the compositions with SBN-rich phase ($0.5 \leq x \leq 0.9$)) led to a continuous reduction of an axial ratio (c/a, c/b and b/a) of SBN, suggesting that ions from the PZT phase substituted in the SBN lattice. Based on the X-ray results, it should be noted that peak shift and the change of axial ratio was observed for the compositional range of $0.1 \leq x \leq 0.9$, implying that all phases present were solid solutions.

Figure 2 displays the variation of phase content of PZT, PNT and SBN in the nominal PZT-SBN ceramics as a function of SBN concentration. Five regions can be distinguished from the phase evolution behaviour in this ceramic system. Phase field I and V represented PZT-based (PZT(s.s.)) and SBN-based (SBN (s.s.)) solid solutions. Two composite regions (II and IV) were also present. Region II ($0.1 \leq x \leq 0.3$) indicated composite ceramics between PZT(s.s.) and PNT phases. It was found that the amount of PZT(s.s.) decreased while that of PNT increased with increasing SBN content up to $x = 0.3$. This suggested that the PZT rapidly dissolved into SBN to form PNT phase. For further addition of SBN up to $x = 0.5$ (region III in Fig. 2), PNT phase became the dominating phase. However, the phase content of PNT could not be determined due to the small number of compositions investigated in this study. In addition, a small amount of 17 wt%SBN was also contained in this region. However, it was noted that
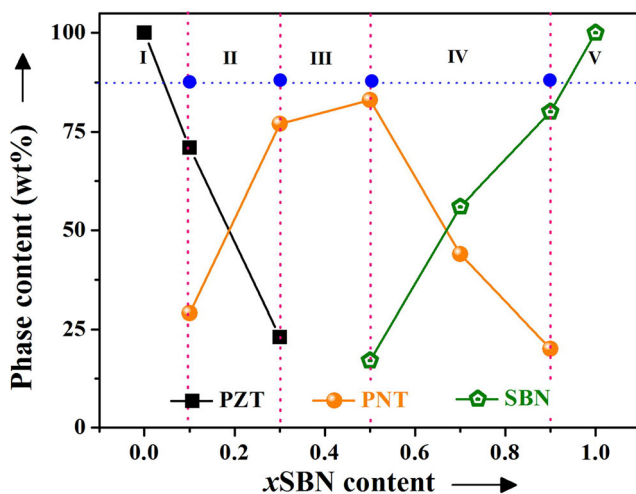
there was no PZT phase in this region. This result demonstrated that a certain amount of PZT preferred to dissolve into SBN structure to form the PNT phase. Furthermore, it can also be said that the SBN phase was a more stable phase than that PZT phase in region III. The region IV ($0.5 \leq x \leq 0.9$) was composed of SBN(s.s.) and PNT phases. In this region, the concentration of SBN phase suddenly increased with increasing SBN addition, whereas the PNT content rapidly decreased. This phase field vs. SBN content plot roughly represented the room temperature stable phase diagram of the nominal PZT-SBN system. It should be noted that the existence of the PNT phase covered a very wide range of compositions ($0.1 \leq x \leq 0.9$), suggesting the stability of this phase as well as the limited solubility of PZT in SBN and vice versa.

SEM micrographs and grain size of the nominal PZT-SBN samples are shown in Fig. 3(a, b), respectively. The shapes and sizes of pure PZT and SBN grains were quite different. As can be seen from Fig. 3(a), the pure PZT ceramic ($x = 0$) had equiaxed grains while the pure SBN ceramic ($x = 1.0$) contained plate shaped grains. For the sample with $0.1 \leq x \leq 0.3$, the ceramic consisted of both equiaxed grains of PZT and irregularly shaped grains of PNT. As the SBN content was increased up to $x = 0.9$, there were two component phases with different shapes and sizes of PNT and SBN in the ceramics. The amount of plate-shaped grains increased gradually while irregularly shaped grains decreased. The variation of grain size for all ceramics are shown in Fig. 3(b). It was interesting to note that the PNT phase formed in this system led to the reduction of the size of the equiaxed grains compared to pure PZT. However, there was little change when compared to pure SBN ceramic. The second PNT particles could inhibit grain boundary migration and limit grain growth in the ceramics. It has also been reported that the presence of a secondary phase can reduce grain sizes of PZT-based ceramics [10].

The room temperature dielectric properties measured at 1 kHz are listed in Table 1. In the case of pure PZT and SBN ceramics, the dielectric constant (ε_r) values were ~1040 and ~175 while the dielectric loss (tan δ) values were ~0.004 and ~0.018, respectively. Starting from pure PZT, the addition of $x = 0.1$SBN caused a sudden increase in the dielectric constant and loss. The smaller grain size of the ferroelectric PZT matrix phase was partly the main contributor to the improved dielectric behavior in this composition due to its greater domain density [11]. Higher domain density also allowed a larger amount of wall movement, thus causing larger dielectric constant and loss observed in the small-grained sample. In addition, the donor-like substitution also played a role in an increase of dielectric constant and loss. Namely, donor-like substitution behavior in which Bi^{3+} substituting for Pb^{2+} and Nb^{5+} for Ti^{4+} or Zr^{4+}. The Bi^{3+} and Nb^{5+} ions from SBN provided extra electrons which could counteract the natural p-type conductivity of PZT ceramic and raise the electrical resistivity [1]. The sample was likely to be charge

Fig. 2 The relationship between phase field and SBN content in PZT ceramic

Fig. 3 (a) SEM images of (1-x)PZT-xSBN ceramics (b) Grain size of nominal (1-x)PZT-xSBN ceramics
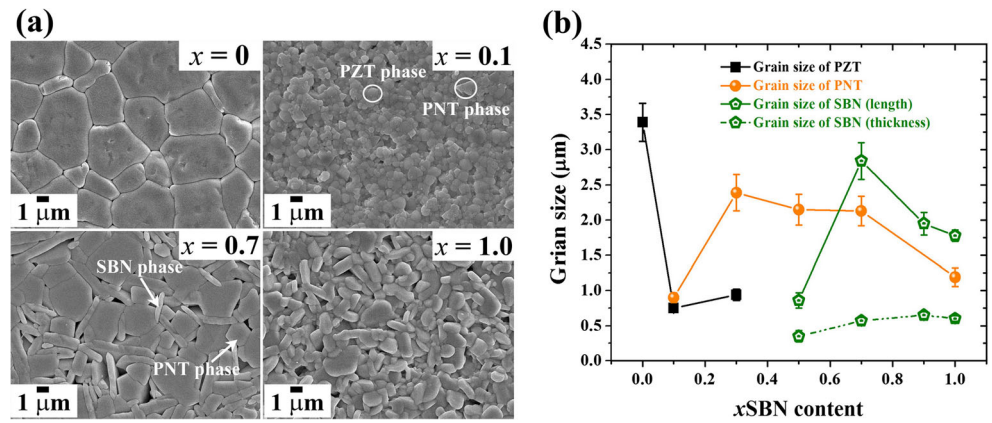
compensated by the formation of cation vacancies such as Pb^{2+} and Ti^{4+} and the released ions then formed the PNT phase observed. On the other hand, the concentration of oxygen vacancies also got significantly reduced [12, 13]. Typically, oxygen vacancies are believed to be a major contributor to domain wall pinning [14]. The reduction of oxygen vacancies led to an enhancement in domain reorientation [15, 16], resulting in high dielectric constant and loss [1]. An increase in SBN content up to $x = 0.7$ caused the dielectric constant and loss of the ceramics to suddenly decrease. This result was attributed to the presence of the non-piezoelectric cubic PNT phase and possibly also to a small amount of some unknown phases, as observed in the X-ray diffraction study. For the composition with $x = 0.9$SBN, the dielectric constant and loss slightly increased. This composition was basically a PZT-doped SBN-based solid solution. However, the small increase in dielectric constant and nearly the same value of dielectric loss compared to pure SBN was not sufficient to indicate with certainty the defect types present in the material. This was made more difficult by the presence of a small amount of PNT secondary phase in this sample.

The polarization-electric field (P-E) loops of nominal (1-x)PZT-xSBN ceramics are shown in Fig. 4. Some ferroelectric parameters extracted from these loops are listed in Table 1. From Fig. 4(a, b), pure PZT ceramic showed larger remanent polarization ($2P_r$) and smaller coercive field ($2E_c$) than pure

SBN ceramic. Addition of $x = 0.1$SBN into the PZT matrix phase led to an increase of the remanent polarization and decrease of the coercive field. This ceramic composition can be a promising material for ferroelectric memory applications due to its high remanent polarization and low coercive field. The increase in the remanent polarization and reduction in the coercive field of the sample was attributed to the effect of donor-like substitution. In this sample, donor dopants (i.e. Bi and Nb from SBN) induced Pb and Ti vacancies in the PZT matrix for charge compensation, and simultaneously reduced the oxygen vacancy content [12, 13]. The reduced oxygen vacancy concentration then contributed to the increase in mobility of domain walls by lowering the stability of domain structure against external electrical field [17], causing the increase of the remanent polarization and reduction of the coercive field. Moreover, the low content of cubic PNT phase also played a role in improving the ferroelectric properties of this composition. For sample with $x = 0.3$SBN, a very slim polarization loop with small remanent polarization and coercive field was present. This was due to an increased amount of cubic PNT phase. Since the cubic PNT phase in the ceramic exhibited non-piezoelectric characteristics, it could obstruct the polarization process of the ferroelectric PZT phase, leading to a reduction of the remanent polarization of this sample. When more SBN ($0.5 \leq x \leq 0.9$) was added to PZT, the P-E loops showed an obvious linear polarization behavior, which

Table 1 Dielectric, ferroelectric and piezoelectric properties of (1-x)PZT-xSBN ceramics

x	Dielectric props.		Ferroelectric props.		Piezoelectric props.		
	ε_r	$\tan\delta$	$2P_r$ ($\mu C/cm^2$)	$2E_c$ (kV/mm)	S_{max} (%)	E_{max} (kV/mm)	d_{33}^* (pm/V)
0	1040.20	0.0043	28.37	3.52	0.17	5.54	320.58
0.1	1799.31	0.0280	39.94	2.86	0.13	4.09	335.18
0.3	761.53	0.0233	4.62	2.82	0.02	8.98	30.12
0.5	165.98	0.0091	-	-	-	-	-
0.7	136.97	0.0031	-	-	-	-	-
0.9	182.40	0.0175	-	-	-	-	-
1.0	174.69	0.0182	5.30	15.73	-	-	-

**Fig. 4** *P-E* loops of (1-*x*)PZT-*x*SBN ceramics, when (**a**) *x* = 0–0.3 and (**b**) *x* = 0.5–1.0
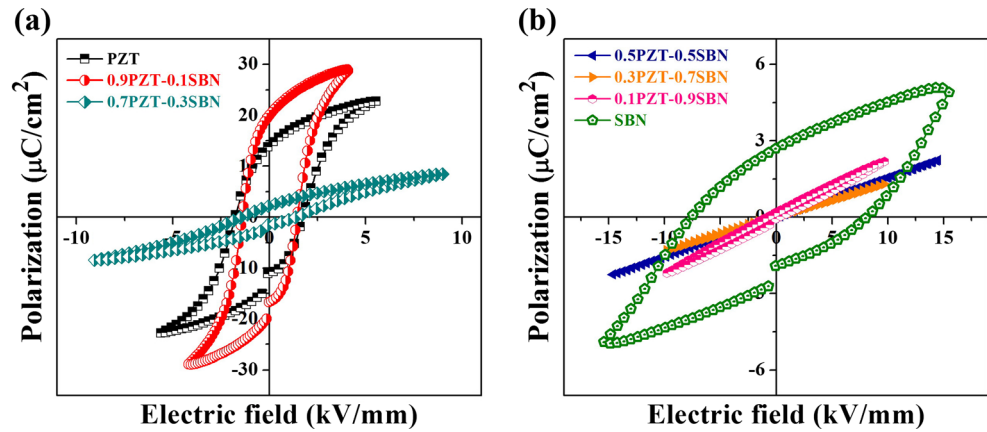
is a characteristic of paraelectric materials [18]. It should be noted that the 0.1PZT-0.9SBN composition also had poor hysteresis loop although this sample was a SBN-rich phase. In this case, the material seemed to exhibit a *p*-type behavior due to that lower valent Pb^{2+}, Zr^{4+}, Ti^{4+} ions substituted into the SBN structure. This led to the formation of oxygen vacancies from charge compensation process. It was expected that the major carrier in this system was holes, implying that this material was a *p*-type semiconductor. The presence of oxygen vacancies obstructed domain reorientation by pinning them, producing a poor hysteresis loop. Over a large compositional range, the presence of the cubic PNT phase obviously led to degradation of the ferroelectric properties of the nominal PZT-SBN system.

The relationships between the field-induced strain (*S*) and the applied external electric field (*E*) for nominal (1-*x*)PZT-*x*SBN ceramics are shown in Fig. 5. The values of the longitudinal piezoelectric constant (d_{33}^*) determined from the slope of strain versus electric field plot [19] are listed in Table 1. From Fig 5(a), the pure PZT ceramic showed a typical butterfly curve with high strain and d_{33}^* values of ~0.17 % and ~320 pm/V, respectively. On the other hand, the pure SBN ceramic showed asymmetric strain loop with very low maximum strain, as shown in Fig 5(b). When a small amount of

0.1SBN was added to PZT, the sample could deliver a field-induced strain of ~0.13 % with at an external electric field of ~4 kV/mm, which was comparable to the strain of undoped PZT. Moreover, the maximum d_{33}^* value was also achieved for this sample (see Table 1). It is well known that the materials for piezoelectric applications are required to possess properties such as high d_{33}^* at low applied electric field [20]. From these results, the piezoelectric properties seemed to be optimized for the 0.9PZT-0.1SBN composition. The donor-doped behavior contributed to the improved piezoelectric properties of this sample. The substitution of Sr^{2+}, Bi^{3+} and Nb^{5+} ions into the PZT introduced the A-site vacancies and also significantly reduced oxygen vacancy concentration. The switching of domains upon electric field application is one of the major mechanisms contributing to the strain response [21, 22]. As mentioned previously, ferroelectric domain walls can be pinned by oxygen vacancies [13]. In this sample, therefore, a decrease in oxygen vacancy concentration resulted in an improvement in ferroelectric domain switching, leading to an increase in strain and corresponding d_{33}^* response. Further increasing SBN content to *x* = 0.3 resulted in a slim butterfly loop with a markedly decreased strain and d_{33}^*. Degradation of the piezoelectric properties in this composition was mainly due to the increased amount of non-ferroelectric

Fig. 5 *S-E* loops of (1-*x*)PZT-*x*SBN ceramics when (**a**) *x* = 0–0.3 and (**b**) *x* = 1.0 (Pure SBN ceramic)
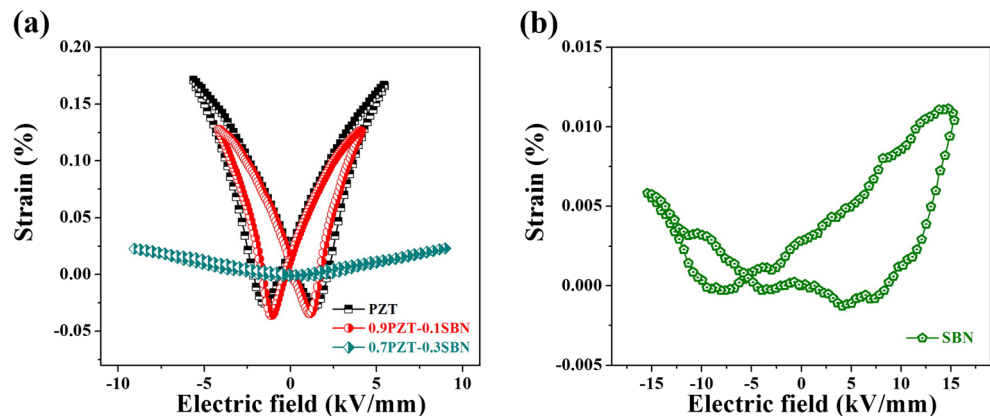
PNT phase. For higher concentration of SBN ($0.5 \leq x \leq 0.9$), no *S-E* loops could be obtained as the strain values were too low and close to the detection limit of the instrument. In addition, the loss of strain response for these ceramics could be caused by the effect of PNT and other unknown phases. These phases might suppress ferroelectric domain switching, causing the loss of strain responses. Therefore, they were not included in Fig. 5. The observed hysteresis loops indicated that these ceramic compositions were neither ferroelectric materials nor exhibited piezoelectric properties. Again, the presence of the non-piezoelectric cubic PNT phase played a major role in the development of the electrical properties of this new material system.

4 Conclusion

($1-x$)Pb(Zr$_{0.52}$Ti$_{0.48}$)O$_3$-xSrBi$_2$Nb$_2$O$_9$ ceramics were successfully prepared by a solid-state mixed-oxide method. The pure PZT ceramic showed mainly tetragonal phase. Addition of small amounts ($0.1 \leq x \leq 0.3$) of SBN into PZT resulted in a tetragonal lattice distortion of the PZT-based solid solution as well as the appearance of a cubic-structured PNT phase. With an increase in the content of SBN, the orthorhombic SBN and the cubic PNT phase were both present in the XRD patterns. This observation suggested that suitable content of added SBN ($x = 0.1$) into nominal PZT-SBN ceramics could improve the electrical properties over those of pure PZT and SBN ceramics. Further increasing SBN content ($x \geq 0.3$) resulted in poor dielectric, ferroelectric and piezoelectric properties. The observed non-piezoelectric secondary phase indicated the high tendency of reaction between PZT and SBN and its presence strongly affected the electrical properties of this material system.

References

1. G. H. Haertling, J. Am. Ceram. Soc. **82**, 797 (1999)
2. K. Miura, Appl. Phys. Lett. **80**, 2967 (2002)
3. D. H. Bao, N. Wakiya, K. Shinozaki, N. Mizutani, J. Phys. D. Appl. Phys. **35**, L1 (2002)
4. K. Amanuma, T. Hase, Y. Miyasaka, Appl. Phys. Lett. **66**, 211 (1995)
5. K. Kato, Jpn. J. Appl. Phys. **37**, 5178 (1998)
6. W. Q. Zhang, A. D. Li, Q. Y. Shao, Y. D. Xia, D. Wu, Z. G. Liu, N. B. Ming, Appl. Surf. Sci. **254**, 1583 (2008)
7. H. H. Park, H. H. Park, T. S. Kim, R. H. Hill, Sensors and Actuat. **B130**, 696 (2008)
8. J. S. Yang, X. M. Chen, T. Aizawa, M. Kuwabara, Solid State Ionics **108**, 117 (1998)
9. R. D. Shannon, Acta Cryst **A32**, 751 (1976)
10. S.-J. Yoon, J.-W. Choi, J.-Y. Choi, D. Wan, Q. Li, Y. Yang, J. Korean Phys. Soc. **57**, 863 (2010)
11. G. Arlt, D. Hennings, G. De With, J. Appl. Phys. **58**, 1619 (1985)
12. K. B. Lee, H. S. Lee, S. K. Cho, J. Korean Phys. Soc. **31**(3), 532 (1997)
13. M. Pereira, A. G. Peixoto, M. J. M. Gomes, J. Eur. Ceram. Soc. **21**, 1353 (2001)
14. W. L. Warren, D. Dimos, B. A. Tuttle, G. E. Pike, H. N. Al-Shareef, Integ. Ferro. **16**, 77 (1997)
15. W. Zhu, I. Fujii, W. Ren, S.T.-McKinstry, J. Am. Ceram. Soc. **95**, 2906 (2012)
16. G. H. Haertling, C. E. Land, J. Am. Ceram. Soc. **54**, 1 (1971)
17. Q. M. Zhang, J. Zhao, K. Uchino, J. Zheng, J. Mater. Res. **12**, 34 (1997)
18. W. Jo, R. Dittmer, M. Acosta, J. Zang, C. Groh, E. Sapper, K. Wang, J. Rödel, J. Electroceram. **29**, 71 (2012)
19. S. Mahajan, O. P. Thakur, C. Prakash, Defence Sci. J. **57**, 23 (2007)
20. S.-T. Zhang, A. B. Kounga, E. Aulbach, H. Ehrenberg, J. Rödel, Appl. Phys. Lett. **91**, 112906 (2007)
21. W. Jo, J. R del, Appl. Phys. Lett. **99**, 042901 (2011)
22. Y. Hiruma, H. Nagata, T. Takenaka, Jpn. J. Appl. Phys **48**, 09KC08 (2009)